Using a Flywheel to Stabilize a Self-Balancing Bicycle

I. I. SILLER-ALCALÁ, J. U. LICEAGA-CASTRO, R. A. ALCÁNTARA-RAMÍREZ
S. CALZADILLA-AYALA
Departamento de Electrónica, Área de Control de Procesos,
Universidad Autónoma Metropolitana,
Av. San Pablo No. 180, Col. Reynosa Tamaulipas, Del. Azcapotzalco, C. P.0200, México D.F.,
MÉXICO

Abstract: - The designs of two linear control systems approach to stabilize the balance of an unmanned bicycle system are presented. Both approaches are based on the use of a reaction wheel or flywheel to balance the bicycle. The two linear control approaches, based on the linearization of a nonlinear model obtained using Lagrange formalism, are the classic linear controllers, PID and State Feedback control. The performance of both controllers is verified by digital simulation and real-time experimental results.

Key-Words: - Reaction Wheel, Balancing control, State feedback controller, Bicycle robot, Classic Control, PID.

Received: March 21, 2023. Revised: January 20, 2024. Accepted: March 9, 2024. Published: April 16, 2024.

1 Introduction

In the last two decades, scientists have focused on achieving the goal of balancing a two-wheeled bicycle. The problem of unmanned balancing the bicycle when it is moving at a certain speed or zero speed is very attractive to systems control researchers, [1], [2], [3], because it presents three interesting problems for this community: the system is unstable, a zero at the origin, and the presence of disturbances. To solve this problem, authors usually use a robust control algorithm and mechanical devices, such as flywheels or gyroscopes, to add them to the bicycle to stabilize it at zero speed wheel, [4], [5], [6], [7], [8], [9], [10], [11], [12], [13], [14], [15], [16]. Although, in this paper, the flywheel could be assumed as a basic gyroscope working only on an axis of rotation, it may be a first step in the use of full gyroscopes, not only as rigid body position sensors but for the stabilization of mechanical vehicles. For instance, gyroscopes could be used as satellite position controllers. However, it requires first designing, controllers for the gyroscopes themselves. Unfortunately, this is not a simple task because gyroscopes are highly nonlinear multivariable systems, [17] and [18].

In this work, the prototype of an autonomous bicycle is stabilized at zero speed, that is, when the bicycle is not moving; so, the bicycle is treated as an inverted pendulum, neglecting the induced torques generated by maneuvering the bicycle handlebar. Nonetheless, these torques could be dumped into the bicycle perturbations. The prototype, the basis of this article, is one of three mechatronic systems that can be assembled using a kit called “Arduino Engineering Kit Rev2” [19], developed by Mathworks and Arduino. The two control strategies selected to stabilize the bicycle are PID and state feedback control. These controllers were chosen due to their easy implementation and because they are well suited for an engineering context. Additionally, the State Feedback controller is a natural option because the prototype allows access to all process states. In this context, the article is divided into the following sections: In Section 2, the dynamic model of the self-balancing bicycle based on the Lagrange formalism, which also includes the actuator electric DC motor, is presented. In Section 3 the design of the PID controller and the State Feedback controller are shown. In Section 4, the performance of the designed controllers is verified through simulations and the implementation of the controller. Finally, in Section 5, the conclusion of the research is presented.

2 Mathematical Model of a Self-balancing Bicycle

In this section, the model of the unmanned bicycle system is presented. The development is based on the principle of the inertial wheel pendulum to obtain simplified Lagrange dynamic equations. Subsequently, the nonlinear differential equations are linearized at an equilibrium point. These linear differential equations are the basis for carrying out the design of the two linear controller approaches. The Bicycle to be stabilized is shown in Figure 1.

Fig. 1: Complete robotic bicycle

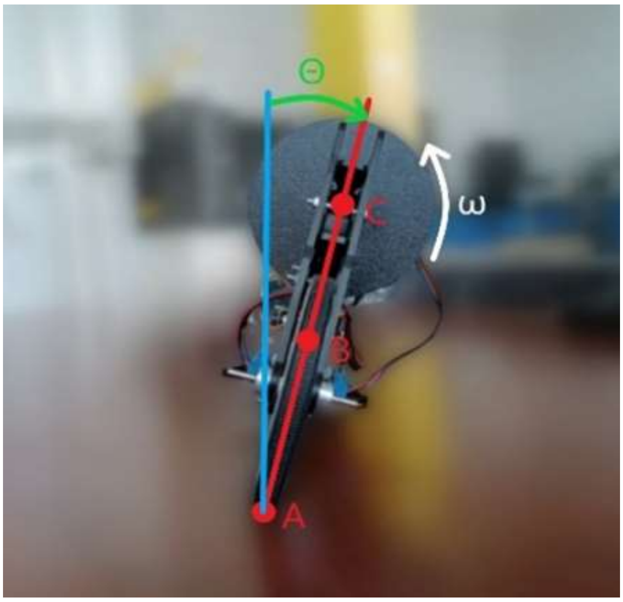

Fig. 2: Front view of the robotic bicycle and reference coordinate system

To obtain the equations describing the dynamics of the system, a behavior like an inverted pendulum with a flywheel is assumed.

The variables and coordinate system that were used are shown in Figure 2, from the front view of the robotic bicycle, where:

θ: It is the angle of inclination of the robotic bicycle concerning the vertical axis.

ω: It is the angular velocity of the flywheel or reaction wheel.

A: It is the axis of rotation of the inverted pendulum, in this case, the robotic bicycle.

B: It is the center of mass of the robotic bicycle.

Table 1. Dynamic Parameters

Parameter	Value
g	9.8067 m/s²
I_b^A	0.00169 kg·m²
I_b^B	0.000445 kg·m²
I_{vi}^A	0.00126 kg·m²
I_{vi}^C	0.00008687 kg·m²
l	0.13 m
l_{AB}	0.065 m
l_{AC}	0.13 m
l_{AD}	0.13 m
m_b	0.2948 kg
m_{vi}	0.0695 kg
r	0.02 m
R	0.05 m
I_B	0.00295 kg·m²
K_m	0.019 N*m/A
K_a	0.019 V*s/rad
R_a	6.48 Ω

First, the model of the electric DC motor actuator is developed. Using the basic circuit that represents a DC motor in Figure 3, the equation below is obtained:

$$V = R_a i_a + L_a \frac{di_a}{dt} + E_a \tag{1}$$

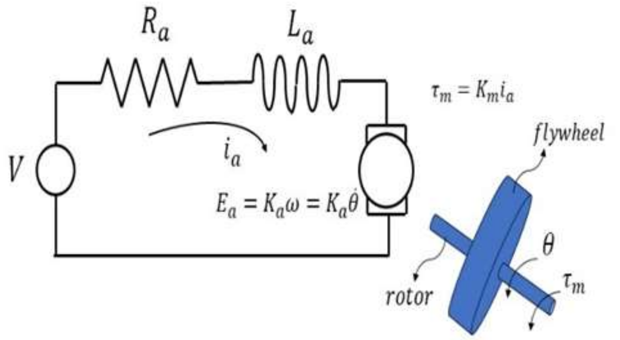

Fig. 3: Diagram of DC motor

Where, V is the motor supply voltage, R_a and L_a are the armature coil resistance and inductance, respectively; i_a is the armature current, and E_a is the counter-electromotive force, given by the following equation:

$$E_a = K_a\omega \tag{2}$$

Where $\omega(t) = \theta'(t)$ is the rotor speed, and therefore, the flywheel angular velocity and, K_a is the electromotive constant. In DC motors, it is generally assumed that the generated torque is proportional to the current provided, this relationship is clarified in the following equation:

$$\tau_m = K_m i_a \tag{3}$$

where $\tau_m(t)$ is the torque generated by the motor and K_m is the torque constant of the motor, the following equation is obtained by substituting (1) into (3).

$$\tau_m = \frac{K_m}{R_a}\left(V - L_a\frac{di_a}{dt} - E_a\right) \tag{4}$$

It is considered that the term corresponding to the inductance L_a can be neglected, since its value is much lower than that of the resistance R_a, considering this and substituting (2) into (4), the following equation is obtained:

$$\tau_m = \frac{K_m}{R_a}(V - K_a\omega) \tag{5}$$

By using the Lagrange formalism, the following equations that describe the mechanical dynamics of the system are given.

The torque about a given axis of rotation is the sum of all the torques that act in the system on this axis, and is defined as:

$$\tau_N = \sum \tau_{si} = I_s\ddot{\theta}_s \tag{6}$$

where,

τ_N : It is the net torque applied to the axis of rotation.

τ_{si} : These are the torques applied on the axis of rotation.

I_s : Moment of inertia of the system.

$\ddot{\theta}_s$: Angular acceleration of the system

If no external torque acts on the robotic bicycle, other than that due to gravitational acceleration, we have two torques that act on the bicycle:

τ_g : Torque due to gravitational acceleration.

τ_{vi} : Torque due to the flywheel.

Therefore, the net torque on the bicycle with respect to the axis of rotation A, Figure 2, results in:

$$\tau_{Bnet} = I_B\ddot{\theta} = \tau_g - \tau_{vi} \tag{7}$$

Where the bicycle's moment of inertia is I_b. The torque τ_{vi}, provided by the flywheel which in turn is generated by the DC motor, must be of equal magnitude but in the opposite direction to the torque τ_g, in such a way that the angular momentum of the robotic bicycle is conserved. Expanding the terms of equation (7) we obtain:

$$I_B\ddot{\theta} = m_b g l_{AB}\mathrm{sen}(\theta) + m_{vi} g l_{AC}\mathrm{sen}(\theta) - I_{vi}^C\dot{\omega} \tag{8}$$

The torque τ_{vi} which is provided by the flywheel can be described by the following equation:

$$\tau_{vi} = I_{vi}^C(\dot{\omega} + \ddot{\theta}) \tag{9}$$

Subsequently, adding equations (5) to (8) and (9), we obtain:

$$I_B\ddot{\theta} = m_b g l_{AB}\mathrm{sen}(\theta) + m_{vi} g l_{AC}\mathrm{sen}(\theta) - \left(\frac{K_m}{R_a I_{vi}^C}(V - K_a\omega) - I_{vi}^C\ddot{\theta}\right) \tag{10}$$

$$\tau_{vi} = 0.5 m_{vi} R^2(\dot{\omega} + \ddot{\theta}) = \tau_m = \frac{K_m}{R_a}(V - K_a\omega) \tag{11}$$

Defining states $x_1 = \theta, x_2 = \theta', x_3 = \omega$, the non-linear state space representation is given by:

$$\begin{bmatrix}\dot{x}_1\\ \dot{x}_2\\ \dot{x}_3\end{bmatrix} = \begin{bmatrix} x_2 \\ \dfrac{m_b g l_{AB} + m_{vi} g l_{AC}}{I_B - I_{vi}^C} sen(x_1) + \dfrac{K_m K_a}{R_a(I_B - I_{vi}^C)}x_2 - \dfrac{K_m}{R_a(I_B - I_{vi}^C)}u \\ -\dfrac{m_b g l_{AB} + m_{vi} g l_{AC}}{I_B - I_{vi}^C} sen(x_1) - \dfrac{K_m K_a I_B}{I_{vi}^C R_a(I_B - I_{vi}^C)}x_3 + \dfrac{K_m I_B}{I_{vi}^C R_a(I_B - I_{vi}^C)}u \end{bmatrix} = \begin{bmatrix} f_1\\ f_2\\ f_3\end{bmatrix}$$

$$y = x_1 = h(x) = [1 \quad 0 \quad 0]\begin{bmatrix}x_1\\ x_2\\ x_3\end{bmatrix} \tag{12}$$

Linearizing the nonlinear equations (12), [20], at the equilibrium point $x^0 = [x_1(0) \quad x_2(0) \quad x_3(0)] = [0 \quad 0 \quad 0]$; $u^0 = u(0) = 0$, the state space representation, where:

$$A = \begin{bmatrix} \frac{\delta f_1}{\delta x_1} & \frac{\delta f_1}{\delta x_2} & \frac{\delta f_1}{\delta x_3} \\ \frac{\delta f_2}{\delta x_1} & \frac{\delta f_2}{\delta x_2} & \frac{\delta f_2}{\delta x_3} \\ \frac{\delta f_3}{\delta x_1} & \frac{\delta f_3}{\delta x_2} & \frac{\delta f_3}{\delta x_3} \end{bmatrix}_{X^0}; \quad B = \begin{bmatrix} \frac{\delta f_1}{\delta u} \\ \frac{\delta f_2}{\delta u} \\ \frac{\delta f_3}{\delta u} \end{bmatrix}_{u^0} u; \quad C = [1 \quad 0 \quad 0]; \tag{13}$$

with $u = V$ is given by:

$$\begin{bmatrix}\dot{x}_1\\ \dot{x}_2\\ \dot{x}_3\end{bmatrix} = \begin{bmatrix} 0 & 1 & 0 \\ \dfrac{m_b g l_{AB} + m_{vi} g l_{AC}}{I_B - I_{vi}^C} & 0 & \dfrac{K_m K_a}{R_a(I_B - I_{vi}^C)} \\ -\dfrac{m_b g l_{AB} + m_{vi} g l_{AC}}{I_B - I_{vi}^C} & 0 & -\dfrac{K_m K_a I_B}{I_{vi}^C R_a(I_B - I_{vi}^C)} \end{bmatrix}\begin{bmatrix}x_1\\ x_2\\ x_3\end{bmatrix} + \begin{bmatrix} 0 \\ -\dfrac{K_m}{R_a(I_B - I_{vi}^C)} \\ \dfrac{K_m I_B}{I_{vi}^C R_a(I_B - I_{vi}^C)} \end{bmatrix} V$$

$$y = [1 \quad 0 \quad 0]\begin{bmatrix}x_1\\ x_2\\ x_3\end{bmatrix} \tag{14}$$

Substituting the values of the parameters provided by the prototype maker, Table 1, we obtain the linear state space model:

$$\begin{bmatrix}\dot{x}_1\\ \dot{x}_2\\ \dot{x}_3\end{bmatrix} = \begin{bmatrix}0 & 1 & 0\\ 96.5795 & 0 & 0.0195\\ -96.5795 & 0 & -0.6608\end{bmatrix}\begin{bmatrix}x_1\\ x_2\\ x_3\end{bmatrix} + \begin{bmatrix}0\\ -1.0241\\ 34.7768\end{bmatrix}V$$

$$y = \begin{bmatrix}1 & 0 & 0\end{bmatrix}\begin{bmatrix}x_1\\ x_2\\ x_3\end{bmatrix} \qquad (15)$$

3 Control Design

In this section, the design of two linear controllers is presented. The PID and state feedback controllers were chosen. Both controllers were chosen mainly because of their well-proven effectiveness, for the PID controller, and because there is complete access to the state vector, in the case of State Feedback. Also, both controllers are easy to implement and are well suited for engineering contexts.

3.1 PID Control Design

The Transfer Function associated with the linear state space model of equation (15) is as follows:

$$G(s) = C(sI - A)^{-1}B = \frac{-1.024s}{(s^3 + 0.6608s^2 - 96.5795s - 61.9366)} \qquad (16)$$

Rewriting the above equation:

$$G(s) = \frac{-1.024s}{(s - 9.818)(s + 9.838)(s + 0.6412)} \qquad (17)$$

The system is unstable, with a pole at 9.818, two stable poles {-9.838, -0.6412}, and a zero at the origin. The root locus of $G(s)$is presented in Figure 4.

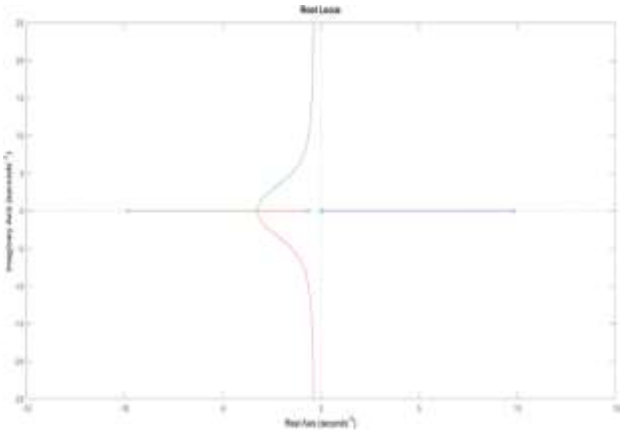

Fig. 4: Root locus of G(s)

One of the closed-loop poles lies on the right half of the S plane, making the system unstable. In addition, there is zero at the origin, which becomes an uncomfortable issue because it represents a derivative behavior in the system and can lead to stabilizing the system using a PID controller.

From the observations made on the graph of the root locus of the system, the following transfer function was designed for the bicycle's PID controller:

$$C(s) = \frac{s^2 + 10s + 30}{s} \qquad (18)$$

The pole at the origin in C(s) has the purpose of removing the origin zero in G(s), while the complex conjugate zeros must be responsible for determining the trajectory of the root locus so that, with an appropriate gain, all the poles will lie on the left-hand plane. The transfer function of the open loop system is given by:

$$G_{LA}(s) = C(s)G(s) = \frac{-1.024s^3 - 10.24s^2 - 30.72s}{s^4 + 0.661s^3 - 96.58s^2 - 61.94s} \qquad (19)$$

The roots of the closed-loop system can be analyzed by using the root locus.

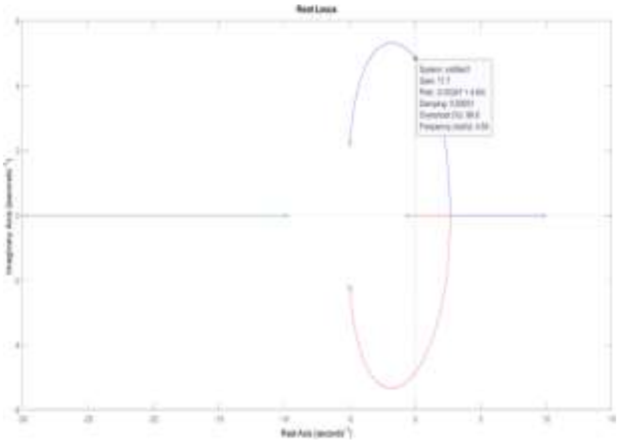

Fig. 5: Root locus of $G_{LA}(s)$

As seen in the graph in Figure 5, when adding the controller, the roots locus changes according to plan, with a gain greater than 11.7, the closed-loop poles will lie in the left half-plane, so the system becomes closed-loop stable. However, the stable closed-loop pole close to the origin, which becomes the dominant pole, may affect the performance of the control system due to its very large steady-state time. Therefore, redesigning the controller to reduce the steady-state time of the dominant poles results in:

$$C(s) = \frac{s^2 + 20s + 104}{0.001s^2 + s} \qquad (20)$$

With this new controller design, the root locus is shown in the following Figure 6.

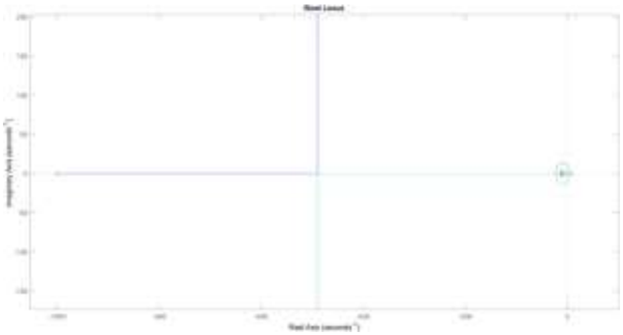

Fig. 6: Root locus with the new controller

In this graph, it is observed that the pole introduced by the controller at -1000 causes one of the poles closest to the origin to move away from the origin and, finally, around -500 together with the high-frequency pole, both poles separate from the real axis symmetrically, resulting in a pair of non-dominant complex poles.

Figure 7 shows a close-up of the trajectories of the dominant poles that are close to the origin.

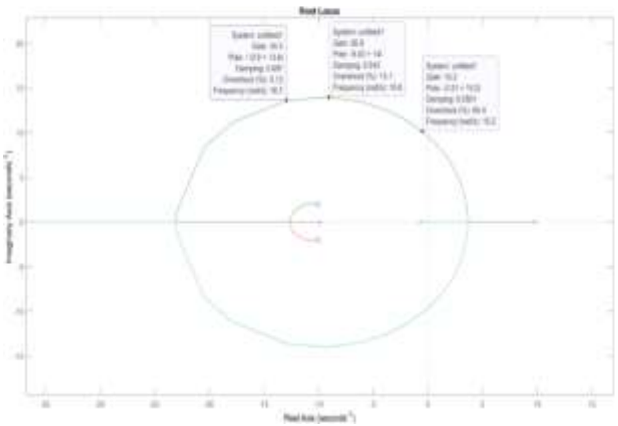

Fig. 7: Root locus close-up with new controller

Finally, a gain of 28 has been chosen so that the poles lie on the left half-plane, thereby ensuring the closed-loop stability of the system.

The Nyquist plot and Bode diagrams of $C(s)G(s)$, shown in Figure 8 and Figure 9, show that robustness is also guaranteed as the stability margins result in $M_g = \infty dBs$ and $M_p = -57$

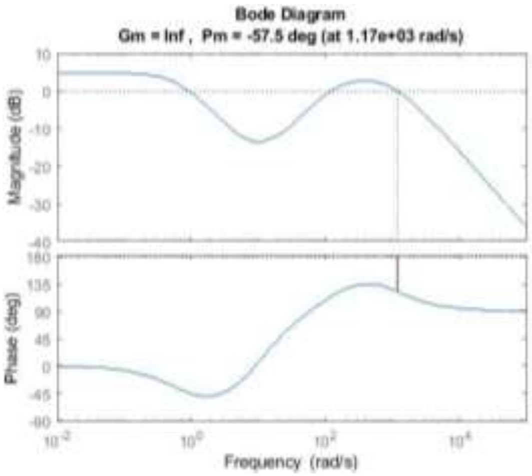

Fig. 8: Bode Diagrams of $C(s)G(s)$

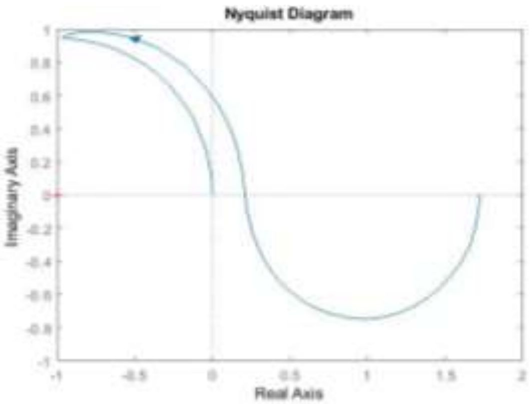

Fig. 9: Nyquist plot of $C(s)G(s)$

To assess the performance of the control system based on the controller of equation (20), the result of a digital simulation based on the nonlinear model of equations (10) and (11), assuming an obvious reference signal of 0° and constant disturbances of $\pm 6°$ with a frequency of 0.5 rad/sec is presented in Figure 10. This figure shows that controller (20) stabilizes the system with excellent disturbance rejection, achieving the objective.

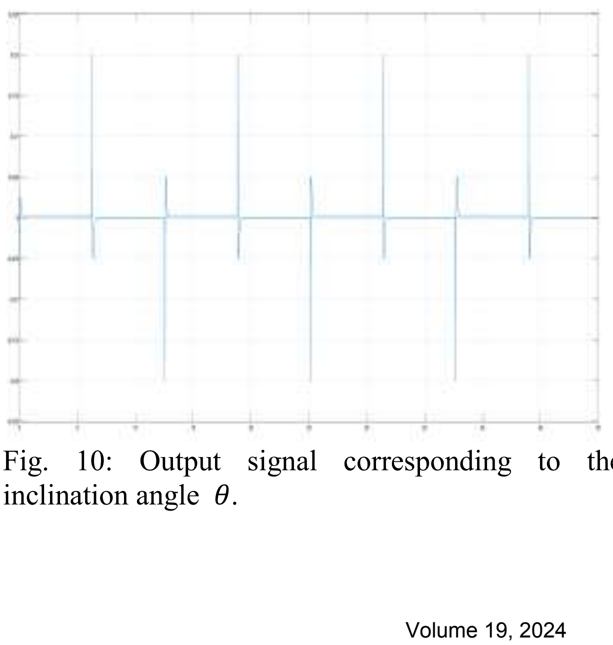

Fig. 10: Output signal corresponding to the inclination angle θ.

Unfortunately, it was not possible to carry out a real-time implementation using the controller of equation (20) as the control system became unstable. This is due to the required pole/zero cancellation at the origin, a cancellation that cannot be guaranteed in practice. Furthermore, as shown in Figure 4, if the controller does not cancel zero at the origin using an integrator or a pole at the origin, an unstable controller would be necessary to break the direct path between the unstable pole at 9.818 and zero at the origin. A possible alternative to an unstable controller is to combine a State Feedback controller with a PI controller, as depicted in Figure 11. The State Feedback controller will stabilize the system, while the PI controller will ensure performance.

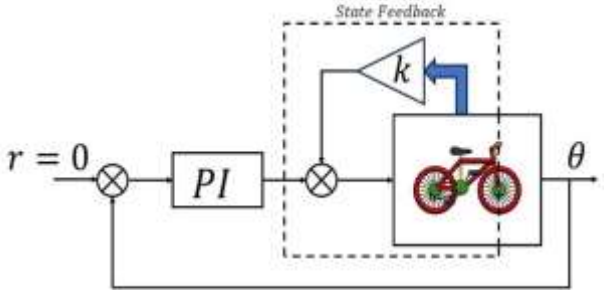

Fig. 11: PI and State Feedback Control System

3.2 Pole Placement State Feedback Control Design

It is well-known that the stability and control performance of a closed-loop system depends on its pole locations. In this section, the pole placement method will be used to place the poles of the closed-loop system in the desired positions by state feedback. To achieve this, the sufficient and necessary condition for the existence of the state feedback controller is that the system must be controllable.

To know if this system, represented by the state equations (14), is controllable, it is necessary to check that the controllability matrix C_M is full range. For this system, the matrix C_M is defined as:

$$C_M = [B \quad AB \quad A^2B] \tag{21}$$

The rank of the controllability matrix is equal to the number of linearly independent rows or columns, therefore, the C_M matrix is full rank, if its determinant is different from zero.

The controllability matrix of this system

$$C_M = [B \quad AB \quad A^2B]= \tag{22}$$

$$\begin{bmatrix} 0 & \frac{K_m K_a}{R_a(I_B - I_{vi}^C)} & \frac{K_m^2 K_a I_B}{I_{vi}^C R_a^2 (I_B - I_{vi}^C)^2} \\ -\frac{K_m}{R_a(I_B - I_{vi}^C)} & \frac{K_m^2 K_a I_B}{I_{vi}^C R_a^2 (I_B - I_{vi}^C)^2} & -\frac{(m_b g l_{AB} + m_{vi} g l_{AC}) K_m {I_{vi}^C}^2 R_a^2 (I_B - I_{vi}^C) + K_m^3 K_a^2 I_B^2}{{I_{vi}^C}^2 R_a^3 (I_B - I_{vi}^C)^3} \\ \frac{K_m I_B}{I_{vi}^C R_a (I_B - I_{vi}^C)} & -\frac{K_m^2 K_a I_B^2}{{I_{vi}^C}^2 R_a^2 (I_B - I_{vi}^C)^2} & \frac{(m_b g l_{AB} + m_{vi} g l_{AC}) K_m {I_{vi}^C}^3 R_a^2 (I_B - I_{vi}^C) + K_m^3 K_a^2 I_B^3}{{I_{vi}^C}^3 R_a^3 (I_B - I_{vi}^C)^3} \end{bmatrix}$$

The determinant is given by:

$$|C_M| = \frac{(m_b g l_{AB} + m_{vi} g l_{AC}) K_m^3}{R_a^3 I_{vi}^C (I_B - I_{vi}^C)^3} = 143.5352 \times 10^3 \tag{23}$$

Since the determinant of C_M is not zero its rank is equal to 3, equal to the order of the system, so the system is controllable and, therefore, state feedback control exists.

The system dynamics given by (15) are used for the design of the linear controllers as follows.

Let the control given by:

$$u = r - \boldsymbol{kx} \tag{24}$$

Where u is the control signal, r is the reference signal, and $\boldsymbol{k}$ is the state feedback gain vector.

The closed loop system is as follows:

$$\dot{x} = (\boldsymbol{A} - \boldsymbol{B}k)x + \boldsymbol{B}r; \; y = \boldsymbol{C}x \tag{25}$$

Rewriting

$$\dot{x} = \boldsymbol{A}_{LC}x + \boldsymbol{B}r; \; y = \boldsymbol{C}x \tag{26}$$

where $\boldsymbol{A}_{LC} = \boldsymbol{A} - \boldsymbol{Bk}$, and the input is the reference r.

The state feedback gain vector should be chosen in such a way that eigenvalues are placed on the desired closed-loop poles.

The position of the closed-loop poles was chosen according to the following equation:

$$(s+10)(s+5)(s+1) = s^3 + 16s^2 + 65s + 50 = 0 \tag{27}$$

That is, with a dominant overdamped closed loop at -1. The two non-dominant poles were chosen trying not to obtain excessive high state feedback gains, as this may render saturation on the system input signal. Therefore, solving equation (28):

$$\det\left[\left(sI - A_{LC}\right)\right] = \det\left[\left(sI - A + Bk\right)\right] = s^3 + 16s^2 + 65s + 50 \tag{28}$$

The state feedback gain vector k obtained is given by:

$$\boldsymbol{k} = [-157.799, -16.1466, -0.03441] \tag{29}$$

In this section, the simulations are presented to show the efficiency of the controller. The following Simulink program simulates the state feedback control system composed by

$$\begin{bmatrix}\dot{x}_1\\ \dot{x}_2\\ \dot{x}_3\end{bmatrix}=\begin{bmatrix}0 & 1 & 0\\ 96.5795 & 0 & 0.0195\\ -96.5795 & 0 & -0.6608\end{bmatrix}\begin{bmatrix}x_1\\ x_2\\ x_3\end{bmatrix}+\begin{bmatrix}0\\ -1.0241\\ 34.7768\end{bmatrix}u$$

$$y=\begin{bmatrix}1 & 0 & 0\end{bmatrix}\begin{bmatrix}x_1\\ x_2\\ x_3\end{bmatrix} and\ u=r-\boldsymbol{kx} \qquad (30)$$

The following figures show the graphs obtained by simulation using the Simulink program in Figure 12. As seen in the graphs of Figure 13, Figure 14, and Figure 15, the simulations of the state feedback control system show good performance. It is also important to notice, from Figure 13 and Figure 14, that title angle θ has an overdamped behavior due to the chosen closed loop poles. Even though the initial conditions were set far from ideal positions. The initial conditions are set in the integrators of the Simulink program in Figure 12. Also, Figure 13 and Figure 14 show that the controller could take the output to $\theta = 0^o$, maintaining bicycle balance and stability, in approximately 4 sec. due to the selected closed loop dominant pole at -1.

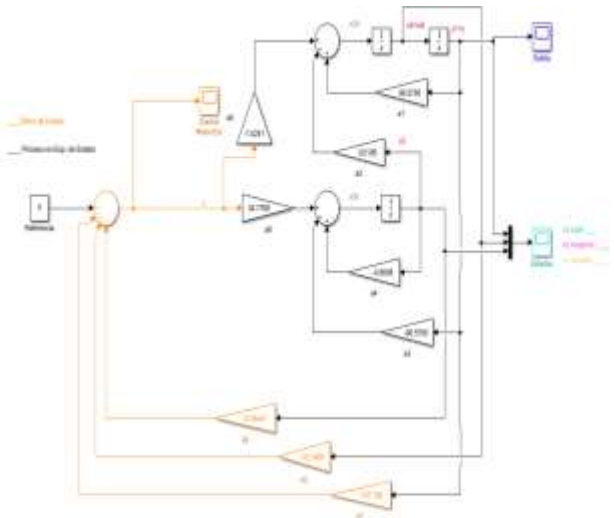

Fig. 12: Simulink program of the bicycle state feedback control system

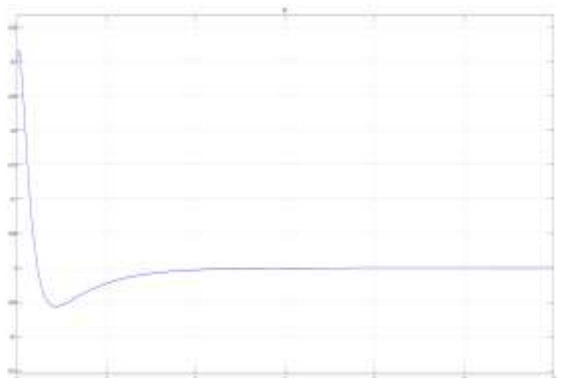

Fig. 13: System output that corresponds to the system inclination angle

In Figure 15, it is observed that the control signal, which represents the voltage that would be applied to the DC motor of the flywheel, has a very large magnitude. This is because the states begin with values far from ideals; that is, to achieve stability and recovery of the bicycle balance does not require a high control effort. Additionally, and as expected, when the bicycle recovers position $\theta = 0°$, the control signal $u \to 0$ so the flywheel velocity tends to zero, Figure 15.

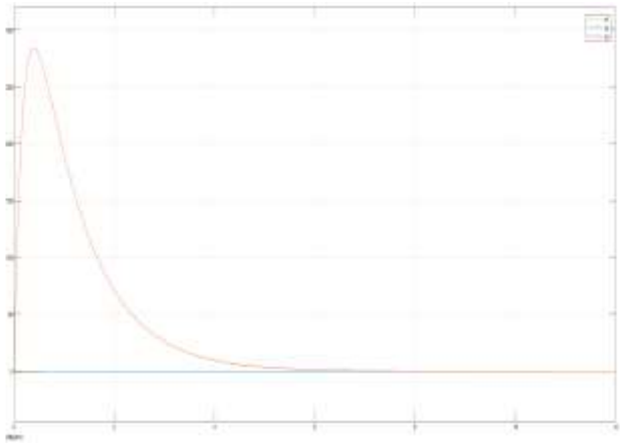

Fig. 14: system states: $x_1 = \theta$ (orange line), $x_2 = \theta'$ (blue line), $x_3 = \omega$ (red line)

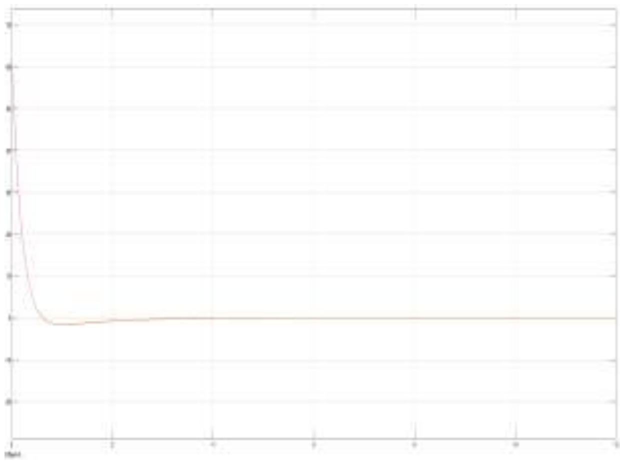

Fig. 15: State feedback control signal

To assess the performance of the state feedback controller, in the presence of output angle variations, with magnitudes that can occur in the real model, an input signal disturbance was added to the diagram in Figure 12 in the state $x_1 = \theta$, which corresponds to the tilt angle of the system, as shown in Figure 16.

The disturbance is a pulse with an amplitude of 0.1745, which would correspond to an inclination of 10°. Furthermore, it occurs 6 seconds after the simulation starts and has a duration of 0.1 seconds.

Below are the graphs of the simulation carried out.

With the results of this second simulation, shown in Figure 17, Figure 18 and Figure 19, it is confirmed that the feedback system behaves correctly, as it was able to reject the perturbation maintaining bicycle verticality. The effort made by the controller, which is observed in Figure 19, is because the disturbance signal is square, but the disturbances or changes in the inclination angle of the real system are not so abrupt, so it was considered that the feedback loop behaves correctly.

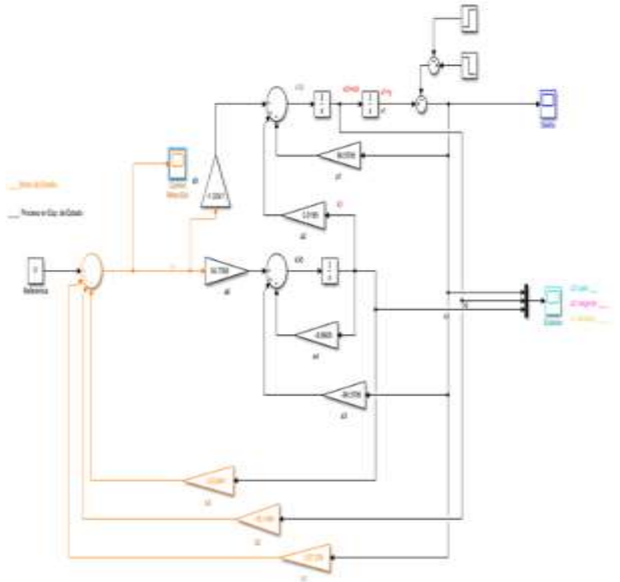

Fig. 16: Simulink diagram of the bicycle state feedback control system with perturbations in state $x_1 = \theta$

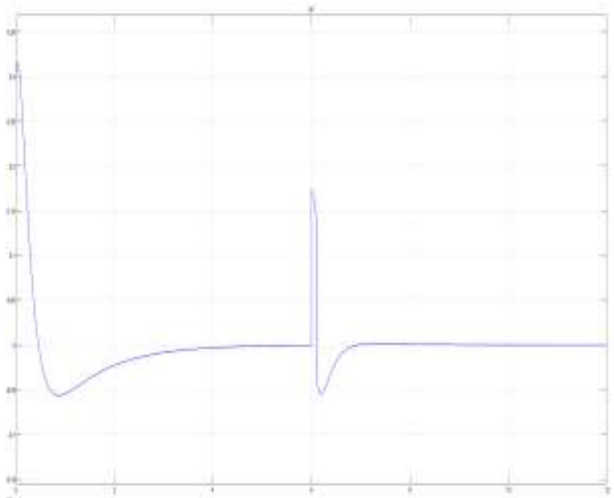

Fig. 17: system output that corresponds to the system inclination angle in the presence of perturbation

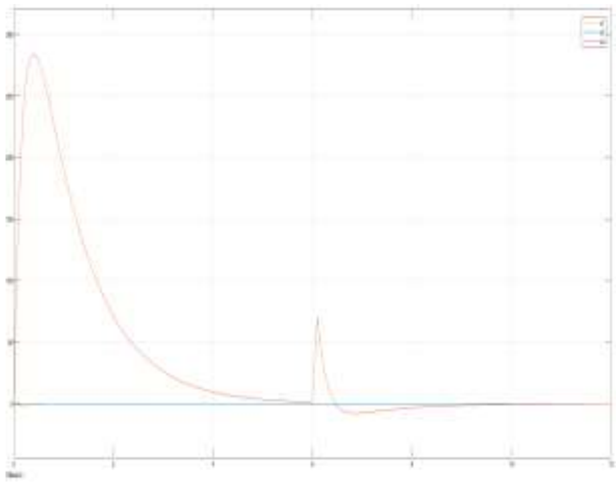

Fig. 18: system states: x1 = θ (orange line), x2 = θ˙ (blue line), x3 = ω (red line) in the presence of perturbation

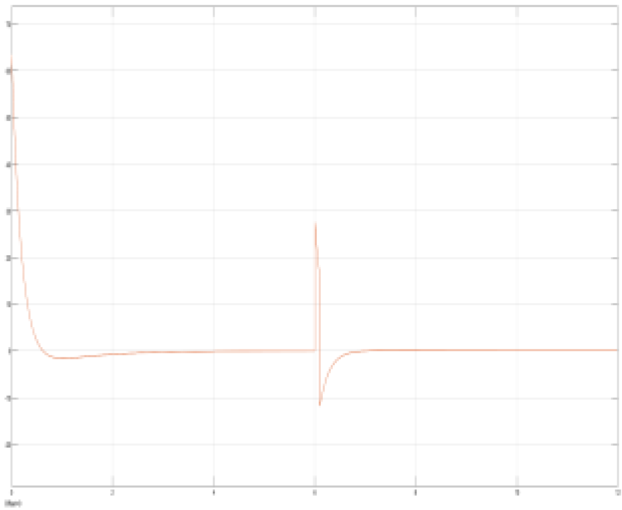

Fig. 19: State feedback control signal in the presence of perturbation

3.3 State Feedback plus PI Control Design

As mentioned above, an alternative to avoid the need to cancel the zero at the origin of the system by using an integrator or a pole at zero in the controller to break the direct path between the unstable pole and the zero, as shown in Figure 4, so that the system is closed loop stable is the combining use of a State Feedback controller with a PI controller. Otherwise, an unstable controller is required.

Following the strategy depicted in Figure 11, the results of a Simulink digital simulations of a control system using the estate feedback vector of equation (29) together with the PI controller of equation (31), are shown in Figure 20, Figure 21 and Figure 22.

$$C_{PI}(s) = \frac{(10s+1)}{s} \tag{31}$$

To better assess the performance of this approach, two perturbation signals were added: a perturbation in the form of a square signal of ± 0.1745, equivalent to $\pm 10°$, with a frequency of $0.25 rad/sec$ on position $x_1 = \theta$, and a random signal with an amplitude of ± 0.05 as sensor noise of $x_1 = \theta$.

From Figure 20, it is clear that the combination of the State Feedback controller and the PI controller presents an excellent response. Moreover, as shown in Figure 21 and Figure 22, the flywheel velocity and control signal are within physical limits. It should be noted that the peak values in the control signal are due to the sudden high perturbations affecting $x_1 = \theta$. Also, the effects of the sensor noise were practically eliminated.

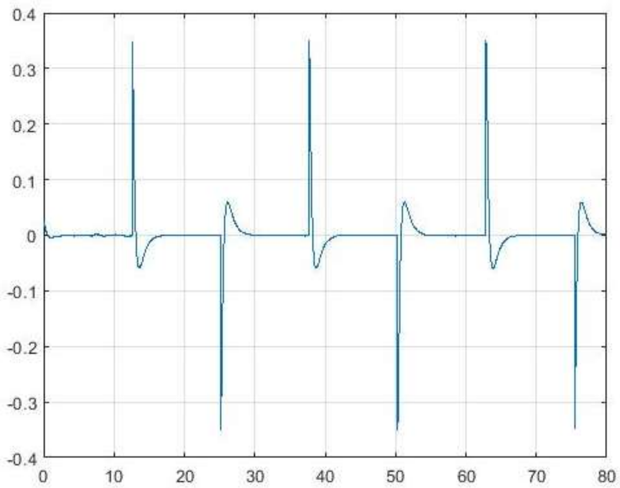

Fig. 20: Tilt or inclination angle θ

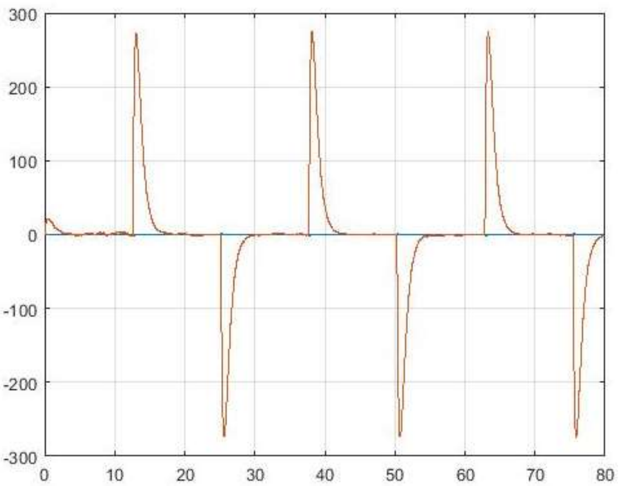

Fig. 21: Tilt angle rate θ' (blue line), ω (red line)

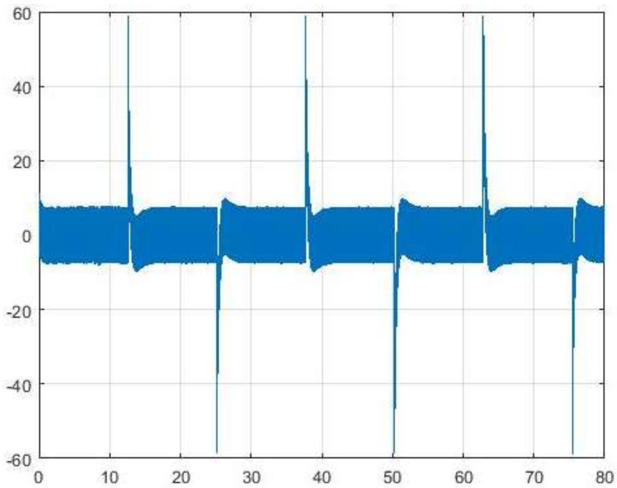

Fig. 22: Control signal $u = V$

4 Implementation of the State Feedback Controller

The software configuration shown in Figure 23 provided by [19], for the operation of the bicycle has the advantage that the state feedback controller designed in this work is easily implemented. The software configuration was developed using Matlab's Simulink, with a sampling time equal to T=0.01.

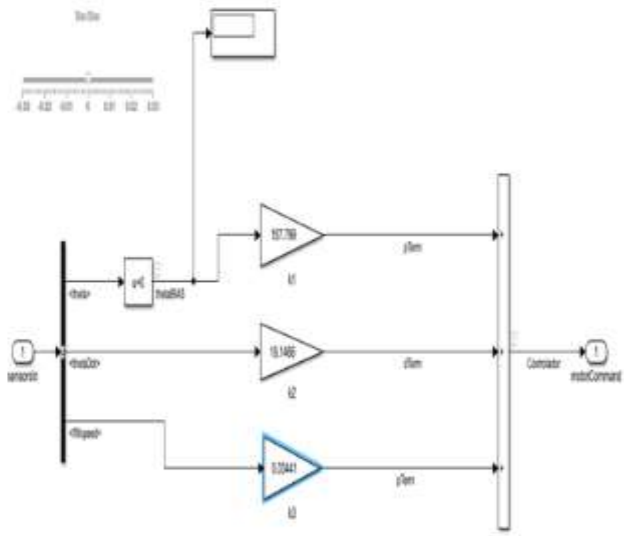
Fig. 23: Implementation of the state feedback controller

It should be noted that the state feedback control was designed based on a continuous state space representation of the system. However controversial, it is possible, in many cases, to implement digitally a controller, designed in continuous time, provided a good sample time is selected, ensuring all system modes are properly sampled, and the digitalized controller does not differ significantly from its continuous counterpart in a range of frequencies well above the control system bandwidth. In this case, the sample period was chosen to satisfy a sampling frequency of 628.32 rad/sec, well above the control system bandwidth of 1 rad/sec.

Figure 24 shows the graphics of the results: inclination angle , inclination angle rate θ' , angular velocity of the flywheel ω, and the control signal produced by the state feedback controller.

Figure 24 shows that the State Feedback controller can maintain bicycle verticality under real-time conditions. That is, with initial conditions far from ideal and sensor noises. This explains the high-frequency components and the almost “chattering” control signal behavior. Excessive control effort could be reduced if dominant closed-loop poles are placed with a longer steady state time, although this could reduce the possibility of reaching stability. That is, the bicycle could lose verticality before the controller has enough time to recover it.

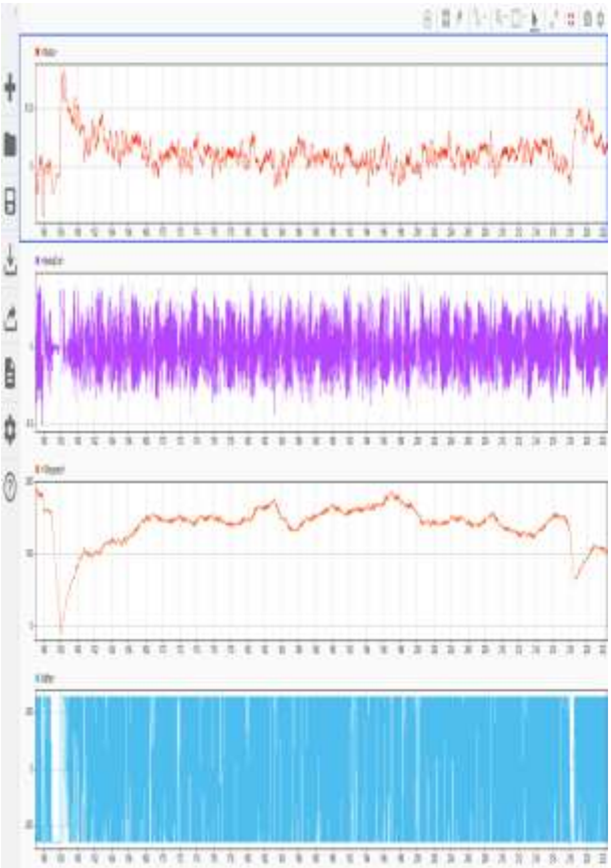

Fig. 24: signals provided by the bicycle sensors while it is balancing: θ (red line), θ' (purple line), ω (orange line), and control signal (blue line)

5 Conclusion

The PID and state feedback controllers were chosen due to the advantages they have, which are: easy implementation, proven robustness and performance, and being well-suited for an engineering context. The implementation of the PID controller could not be carried out, due to the cancellation of the system zero at the origin; that is, the exact pole/zero cancellation at zero cannot be guaranteed due to the approximation of the integral action in the digital implementation of the PID controller, obtaining an unstable response. It is important to recall that stability margins are valid provided there are no open-loop pole/zeros cancellations. That is, Nyquist stability criteria cannot cope with no controllable or no observable systems, a phenomenon occurring under pole/zero cancellation. Further analysis or a more complex linear controller is required to avoid canceling the process zero at zero, for instance, the combination of a State Feedback plus PI control scheme. On the other hand, the state feedback controller has excellent behavior without the need for cancellations. Although it does not include an integral action, it achieves the desired outputs because the signal reference is $r = 0$ and the state feedback assures exponential and asymptotic stability in all the states so, $x_1 = \theta \rightarrow 0$. Therefore, the bicycle maintains verticality.

Nevertheless, and taking advantage of having access to the entire state vector, it would be advisable to design and implement a non-linear state feedback control such as a "Back Stepping" control. In this way, a more direct control could be designed for each state. However, as shown by equations (10), (11), and (17) this may not be a simple task as the system degree is 3 while its relative degree is 2. Also, Sliding Mode control with “super twist” could be analyzed.

References:

[1] Prashant Govardhan, Akhilesh Thakre, Nehal Shende, Nachiket Phadnis, Sudarshan Muley, Survey on self-balancing two-wheel electric prototype, *International Journal of Engineering Research and General Science*, Vol.5, Issue 5, September-October, 2017, pp. 32-36.

[2] Chiu, Chih-Hui, and Chi-Yuan Wu, Bicycle robot balance control based on a robust intelligent controller, *IEEE Access,* Vol.8, 2020, pp. 84837-84849.

[3] Long Chen, Bin Yan, Hai Wang, Ke Shao, Edi Kurniawan, Guangyi Wang, Extreme-

learning-machine-based robust integral terminal sliding mode control of bicycle robot, *Control Engineering Practice*, Vol.12, 2022, pp. 1-10.

[4] Park, S. H., & Yi, S. Y., Active balancing control for unmanned bicycle using scissored-pair control moment gyroscope, *International Journal of Control, Automation and Systems*, Vol.18, 2020, pp. 217-224.

[5] Liu, Y., Jin, Z., Huo, B., Guan, Q. and Yu, H., Self-balance Control of Bicycle with Inertial Wheel Pendulum based on Linear ADRC, 2022 *China Automation Congress*, Xiamen, China, 2022, pp. 6403-6408.

[6] Deng Wenhao, Skyler Moore, Jonathan Bush, Miles Mabey, Wenlong Zhang, Towards automated bicycles: Achieving self-balance using steering control, *The ASME 2018 Dynamic Systems and Control Conference*, Atlanta, Georgia, USA, Vol.2, 2018.

[7] Yongli, Zhang, Yu Liu, and Guorong Yi, Model analysis of unmanned bicycle and variable gain LQR control, *2020 IEEE 9th Joint International Information Technology and Artificial Intelligence Conference (ITAIC)*. Chongqing, ChinaVol.9, 2020, pp. 1196-1200.

[8] He, Ning, Qianhou Hua and Jiaxuan Chen, Self-Balancing Bicycle Based on Control Moment Gyroscope, *42nd Chinese Control Conference (CCC)*. IEEE, Tianjin, China, 2023, pp. 4493-4498.

[9] He, Sihan, Junhao Zeng, and Yisheng Guan, Self-balance Control of an Essboard-like Robot with a Flywheel, *2022 IEEE International Conference on Mechatronics and Automation (ICMA)*, Guilin, Guangxi, China, 2022, pp.110-115.

[10] N. Marios Patsouras, Modelling and control of a self-balancing motorcycle, *Diploma Thesis, University of Thessaly, School of Engineering*, Department of Mechanical Engineering, Greece, 2022.

[11] R. Lot and J. Fleming, Gyroscopic stabilisers for powered two-wheeled vehicles, *Vehicle System Dynamics*, vol. 57, 2019, no. 9, pp. 1381–1406.

[12] VU, Ngoc Kien; NGUYEN, Hong Quang, Balancing control of two-wheel bicycle problems, *Mathematical Problems in Engineering*, 2020, vol. 2020, p. 1-12.

[13] Park J-H, Cho B-K., Development of a self-balancing robot with a control moment gyroscope, International Journal of Advanced Robotic Systems, Vol. 15, 2018, 15(2).

[14] A. Sikander and R. Prasad, Reduced order modelling-based control of two wheeled mobile robot, *Journal of Intelligent Manufacturing*, ol. 30, no. 3, pp. 1057–1067, 2019.

[15] Y. Huang, X. Zhou, Z. Liang and Q. Qin, Design of balanced bicycle system based on anti-integral saturation and incomplete differential PID algorithm, *2023 2nd Asia Conference on Electrical, Power and Computer Engineering (EPCE)*, Xiamen, China, 2023, pp. 94-98.

[16] Zheng, Xudong, Xianjin Zhu, Zhang Chen, Yiyong Sun, Bin Liang, and Tianshu Wang. "Dynamic modeling of an unmanned motorcycle and combined balance control with both steering and double CMGs." *Mechanism and Machine Theory* 169 (2022): 104643.

[17] J. Liceaga C., Jesús and Amézquita B. Luis, Analysis and Modelling of a Gyroscope, *Proceedings of the Seventh IASTED International Conference, Control and Applications*, May 18-20, 2005, Cancún, México.

[18] J. Liceaga, E. Liceaga, and L. Amézquita, Multivariable Gyroscope Control by Individual Channel Design, *Control System Society. Conference on Control Applications 2005*, Toronto, Canada.

[19] Arduino Education, (2021), Arduino Engineering Kit Rev2, Arduino Education, [Online]. https://store-usa.arduino.cc/products/arduino-engineering-kit-rev2?queryID=undefined&selectedStore=us, (Accessed Date: September 18, 2023).

[20] Alberto Isidori, *Non-Linear Control Systems*, Springer, London, 3rd Edition, 1995, ISBN: 978-3-540-19916-8.

Contribution of Individual Authors to the Creation of a Scientific Article (Ghostwriting Policy)

- I. I. Siller-Alcalá carried out the simulation and the control design.
- J. U. Liceaga-Castro carried out the bike model and the control design.
- R. A. Alcántara-Ramírez has organized and executed the experiments.
- S. Calzadilla-Ayala was responsible for the implementation of the controllers.

Sources of Funding for Research Presented in a Scientific Article or Scientific Article Itself

No funding was received for conducting this study.

Conflict of Interest

The authors have no conflicts of interest to declare.